Well-Aligned TiO₂ Nanotube Arrays with Ag Nanoparticles for Highly Efficient Detection of Fe³⁺ Ion

Zong-Min Ma[1,2*], Xing-Sheng Wu[1,2], Dou-Dou Zheng[1,2], Jiu-Yan Wei[1,2], Yan-Na Xie[1,2], Yun-Bo Shi[1,2], Kun Huang[2], Xiao-Ming Zhang[1,2] and Jun Liu[1,2*]

Abstract

Nowadays, determination of the iron ions with high sensitivity and selectivity with novel methods becomes a matter of urgency for monitoring healthy body and environment. In this paper, for the first time, we present a set of high-performance TiO₂ nanotube arrays which are quite sensitive to iron ions. Firstly, the anodic oxidation method was adopted to prepare ordered TiO₂ nanotube arrays, followed by functionalized Ag nanoparticle deposition with the enhancement ability in iron ion sensing. Besides, the spectrum of the TiO₂ nanotube with/without the Ag nanoparticles was analyzed with an X-ray photoelectron spectrometer, which shows that Ag nanoparticles can effectively reduce the recombination rate of electrons and holes, and increase the conductivity and the charge transfer rate of the electrodes. Further, when functionalized Ag nanoparticles on well-ordered TiO₂ nanotube arrays were used, iron ion sensing performed with the anodic stripping voltammetry method was investigated to validate the great potential of TiO₂ nanotube arrays with a sensitivity of approximately 30 μA/ug/L in becoming Fe³⁺ sensors. This method creates new possibilities for developing sensors for monitoring of Fe³⁺ in biological samples without any sample pretreatment procedure.

Keywords: TiO₂ nanotube arrays, Fe³⁺ detection, Functionalized Ag nanoparticle deposition

Background

Iron is an important nutrient element for human health, which is usually responsible for transfer and transport of oxygen and block materials, and ranks second among the most essential metal elements in the human body. However, an excessive amount of iron ions in a living cell can catalyze production of reactive oxygen species (ROS) via the Fenton reaction, which can lead to diseases, such as kidney disease, and disturb the cellular homeostasis resulting in Alzheimer's, Wilson's, and Menkes diseases [1, 2]. As a matter of fact, due to its wide application in industry and agriculture, the potential toxic effects of iron from contaminated rivers, lakes, or oceans on humans remain a global challenge [3, 4]. Consequently, it is particularly

necessary to monitor healthy body and environment to develop practical and efficient technologies used for rapidly determining the iron ions with high sensitivity and selectivity.

Nowadays, there are many methods for detecting metal ions, such as atomic absorption spectrometry, inductively coupled plasma mass spectrometry, and inductively coupled plasma emission spectrometry. However, complicated equipment and sample preparation steps are needed in these methods, which will also result in a large cost. Recently, an enormous effort has been made to studies on nanoparticles, such as graphene [5–12], graphene quantum dots [13–18], carbon dots [19–21], and noble metal nanoparticles or nanoclusters in the desired dimension for sensing of metal ions, which have attracted much attention because of good selectivity, high sensitivity, and easy operation. Vinod Kumar Gupta et al. have developed a method for synthesizing imine through a simple condensation reaction and exploring their metal detection abilities through electrochemical and optical methods. Fe³⁺ detected by

* Correspondence: mzmncit@163.com; liuj@nuc.edu.cn
[1]Science and Technology on Electronic Test & Measurement Laboratory, North University of China, No.3, Xue Yuan Road, Taiyuan 030051, Shanxi, China
Full list of author information is available at the end of the article

Ma *et al. Nanoscale Research Letters*   (2019) 14:49

Page 2 of 8

colorimetric (L2) at a low concentration can reach 1.29×10^{-6} M. But this method is limited due to factors such as high detection limits, and strong interference [22]. Xiaohui Gao et al. reported a facile colorimetric sensor based on the N-acetyl-L-cysteine (NALC)-stabilized Ag nanoparticles (NALC–Ag NPs) for detection of Fe3+ ions in aqueous solution. This method can be used to perform sensitive and selective detection of Fe^{3+} ions in water with a linear range from 80 nM to 80 mM and a detection limit of 80 nM [23]. Kailasa S K et al. have developed a selective and sensitive colorimetric method for determination of Fe^{3+} ion by using p-amino salicylic acid dithiocarbamate functionalized gold nanoparticles (DTC-PAS-Au NPs) as colorimetric probes [24, 25]. On the basis of such detection, inductively coupled plasma (ICP) analysis coupled with mass spectrometry (MS) or optical emission spectroscopy (OES) was preferably adopted for iron ion analysis [26].

On the other hand, TiO_2 nanotubes, with high chemical stability, are widely applied in various industries due to their excellent photo-electrochemical, catalytic, and adsorption properties as well as nontoxicity, such as gas/moisture sensors [27], photocatalytic decomposition of water into hydrogen [28], photocatalytic degradation of organic pollutants [29], dye-sensitized solar cells [30], biosensors [31], and supercapacitors [32]. Particularly, well-structured and highly ordered TiO_2 nanotubes are well suitable for directional and rapid transfer of electrical charges [33–36]. Further, surface functionalization of Ag NPs plays a crucial role in increasing analytical applicability for TiO_2 nanotubes detection of trace analytes with high selectivity and sensitivity. Hence, considering combination of TiO_2 nanotubes and metal ion detection at trace level is highly desirable. As far as we know, there are very few reports on usage of functionalized TiO_2 nanotubes as based probe for Fe^{3+} detection.

In this paper, a set of high-performance TiO_2 nanotube arrays which are quite sensitive to iron ions are presented. Firstly, the anodic oxidation method was adopted to prepare ordered TiO_2 nanotube arrays, followed by functionalized Ag NPs with the ability of iron ions sensing. Besides, the spectrum of the TiO_2 nanotube with/without the Ag NPs was analyzed with an X-ray photoelectron spectrometer. Further, iron ion sensing with the use of functionalized Ag NPs on well-ordered TiO_2 nanotube arrays through the anodic stripping voltammetry method was investigated to validate the great potential of heavy metal sensors of TiO_2 nanotube arrays. This method creates new possibilities for developing sensors for monitoring Fe^{3+} in biological samples without any sample pretreatment procedure.

Methods

Principles of Sensing Iron Ions with TiO_2

The electrons will overcome the bandgap and transit from the valence band (VB) to the conductance band (CB) when absorbing enough energy in TiO_2 nanotube. As a result, there will be a non-occupied electronic state (hole) in VB, which is positive, as explained in Fig. 1a. In this process, when an electron is excited from the VB to the CB, it can diffuse to the surface allowing charge transfer to an adsorbate or can become trapped within an electron trap in the band gap. If the surface of the nanotubes was covered by metal nanoparticles, charge transfer will occur between the adsorbate and the TiO_2 nanotube because of electron transition. Based on this transfer, the amount of metal nanoparticles can be known when the quantity of electric charge is detected, as shown in Fig. 1b and Eqs. (1)–(3). From these equations, it can be seen that the excess charge distribution defines the potential that attracts the electron-withdrawing (O_2) and repels the electron-donating (H_2O) molecules to O_b vacancy defects when metal particles are adsorbed on the TiO_2 surface. Therefore, we can detect the concentration and species of metal nanoparticles directly by measuring the amount of charge transfer with the following equations [37]:

$$\text{Ti}_{(6c)}\left[(4s)^2(3d)^2 \text{ of Ti}_{(6c)}\right] = 4 \times \left[\text{O}_{(3C)}\right] + 2 \times \left[\text{O}_{b(2C)}\right] \tag{1}$$

$$\left[(4s)^2(3d)^2 \text{ of Ti}_{(6c)}\right] + \left[(1s)^1 \text{ of H}\right] = 4 \times \left[\text{O}_{(3C)}\right] + 1 \times \left[\text{O}_{b(2C)}\right] + [\text{OH}] + e^- \tag{2}$$

$$\text{Ti}_{(5c)}\left[(4s)^2(3d)^2 \text{ electrons of Ti}_{(5c)}\right] = 5 \times \left[\text{O}_{(3C)}\right] \tag{3}$$
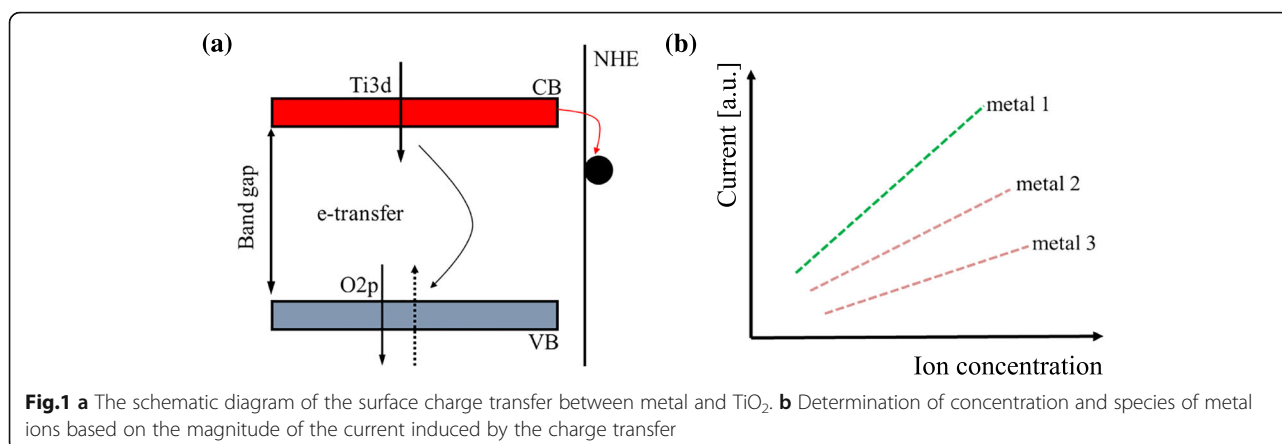
The stripping voltammetry method can be used to identify the concentration and species of metals on the surface of TiO_2 nanotube arrays. In this method, the current's dependence on the concentration and species of metals can be shown in Eq. (4) [38]:

$$\Delta i_p = \frac{nFAD^{1/2}C}{\sqrt{\pi t_m}}\left(\frac{1-\sigma}{1+\sigma}\right) \tag{4}$$

Where, $\sigma = \exp[(nF/RT)(\Delta E/2)]$, and N is the number of electrons participating in reactions with metals. F, A, D, C, and t_m represent Faraday constant, area of the electrode, diffusion coefficient, and the concentration of the metal ions, and pulse width respectively. It can be seen from this equation that the current is proportional to metal concentration.

Experimental Details

A pure titanium sheet ($20 \times 20 \times 0.1$ mm; purity 99.9%) was chemically polished to remove the oxide layer and create a smooth surface. To be specific, a proper amount of HF acid with a concentration of 40% was

Fig.1 a The schematic diagram of the surface charge transfer between metal and TiO_2. **b** Determination of concentration and species of metal ions based on the magnitude of the current induced by the charge transfer

poured into ionized water proportionally (0.5%); then, the titanium sheet was dipped into the pre-prepared solution for 10 s and was taken out instantly and then dried with nitrogen. Next, it was ultrasonically washed in acetone, absolute ethyl alcohol, and deionized water at 30 °C for 12 min respectively. In the process, acetone was mainly used to clean the surface of the Ti sheet with a roughness of 0.139 μm and 0.066 μm before and after the treatment, respectively. Pretreatment of the Ti sheets is necessary prior to experiments for higher smoothness. The experimental setup was applied in Ref. [39]. The AMICUS X-ray photoelectron spectrometer (XPS) from Shimadzu was used for quantitative composition definition of the prepared TiO_2 nanotube arrays.

Ag nanoparticles (NPs) with various sizes were deposited onto the TiO_2 nanotubes surface (QPrep400, Mantis) with the power of 60 W under vacuum conditions of 10^{-3} Torr. Purity of the Ag plate was 99.9999%.

An electrochemical workstation (CHI660E, Shanghai Chenhua) was used to perform the stripping voltammetry experiments for detecting the concentration of Fe^{3+} ions. A three-electrode system (working, reference electrode, and auxiliary electrodes) which is consisted of two loops was used to monitor the electrochemical reaction process of the working electrode and to keep the equilibrium of the chemical reaction.

In the experiments, four types of Fe^{3+} with the concentrations of 10 μg/L, 20 μg /L, 30 μg/L, 40 μg/L, and 50 μg/L were mixed in ammonium chloride, respectively. When detected, neutral iron firstly was adsorbed onto the TiO_2 nanotubes surface with/without Ag deposition after reduction reaction with Ti substrate, followed by re-oxidized when reverse bias was applied. The scanned voltage ranged from − 1 V to 1 V with a step of 0.005 V. The minimum detectable current was 10^{-5}A, and the detected duration was 120 s. Concentration of Fe^{3+} ions was evaluated from the dissolution current peak's dependence on voltage.

Results and Discussion

Preparation and Characterization of TiO₂ Nanotube Arrays

TiO_2 nanotube arrays produced in electrolyte composed of glycol, 2 vol% water and 0.3 wt% ammonium fluoride with the oxidation voltage being 60 V, the oxidation time being 2 h, the oxidation temperature being 40 °C, and the calcination temperature being 500 °C had the optimal morphology and performance [39]. Topography and side-view scanning electron microscope (SEM) images of the TiO_2 nanotube arrays are shown in Fig. 2a, b, respectively. In Fig. 2a, the TiO_2 nanotube arrays are well-arranged with an average diameter of 50 nm. In Fig. 2b, length of the nanotube is approximately 19.2 μm with a relative tilted angle of 30° with substrate when measured. From these results, it can be seen that the contact area with Fe^{3+} ions for the nanotube arrays can be obviously increased as length of the tube increases, which can improve detection sensitivity effectively.

Figure 3a–d shows SEM images of TiO_2 nanotubes with Ag nanoparticle deposition with durations of 30 s, 35 s, 40 s, and 45 s respectively. In Fig. 3a, when deposition duration was 30 s, the average diameter and coverage thickness of the Ag nanoparticles adsorbed on the wall of the nanotubes were approximately at 10 nm and 5 nm respectively. From these results, it can be seen that the nanoparticles are uniform in size distribution. In Fig. 3b, c, when deposition durations were extended to 35 s and 40 s, state of Ag nanoparticles became cluster state gradually and diameters of the Ag particles increased to 20 nm and 25 nm respectively. Diameters of the Ag nanoparticles further increased until they became clusters that partially cover the surface of the TiO_2 nanotube when the deposition time increased to 45 s, which is shown in Fig. 3d.

In order to confirm composition of the TiO_2 nanotube arrays with/without Ag particle adsorption with a duration of 30 s, XPS experiments were performed,
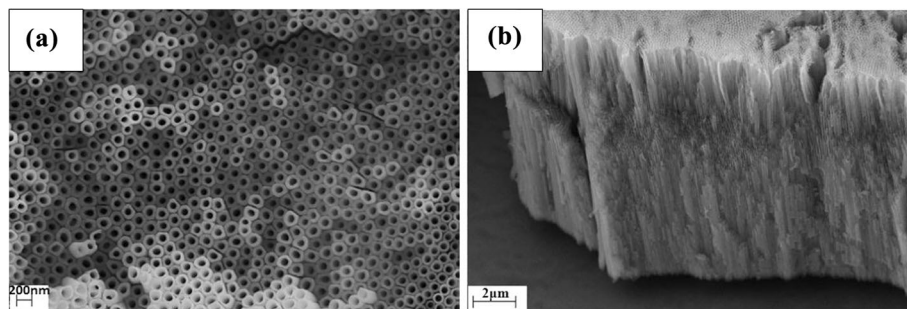
Fig. 2 Topography (**a**) and Side-view (**b**) Images of the TiO$_2$ Nanotube Arrays, respectively

which are shown in Fig. 4a–d. In Fig. 4a, the spectra of Ag were given with the intensities of 3200 and 2400 counts when the values of binding energy were 368.24 eV and 374.25 eV, respectively, which showed that FWHM (full wave at half maximum) of Ag was approximately 1 eV. From this results, it can be seen that only one chemical state Ag^0 was detected after Ag deposition.

In Fig. 4b, spectra of Ti with/without Ag deposition were given and marked with red and black lines. Before Ag deposition, the observed values of binding energy of Ti were 459.60 eV and 465.18 eV with the intensities being 2250 and 1250 counts, respectively. In contrast, the values of binding energy of Ti were 458.88 eV and 464.66 eV with the increasing intensities being 3250 and 2700 counts respectively after deposition. The difference in binding energy before Ag deposition was 5.58 eV; in contrast, the difference after deposition changed to 5.78 eV, which was increased by 0.3

eV approximately. Besides, the two titanium peak shifts were 0.72 eV and 0.52 eV respectively. This phenomenon was caused by the interaction of Ag NPs.

Similar phenomena were observed on the spectra for oxygen and carbon with/without Ag deposition, which are shown in Fig. 4c, d respectively. Before deposition, the values of binding energy of oxygen were 530.89 eV and 533.28 eV with the intensities being 3500 and 4500 counts, respectively. These results showed that the oxygen was in a negative two-valence state (lattice oxygen) and consisted of TiO$_2$ with titanium. On the other hand, the value of binding energy of oxygen was 530.24 eV with the intensity being 4900 counts after deposition. Besides, the value of oxygen peak of binding energy, 533.28 eV, disappeared after deposition, and the oxygen peak shift was 0.67 eV. These results demonstrated that the state of oxygen was changed from
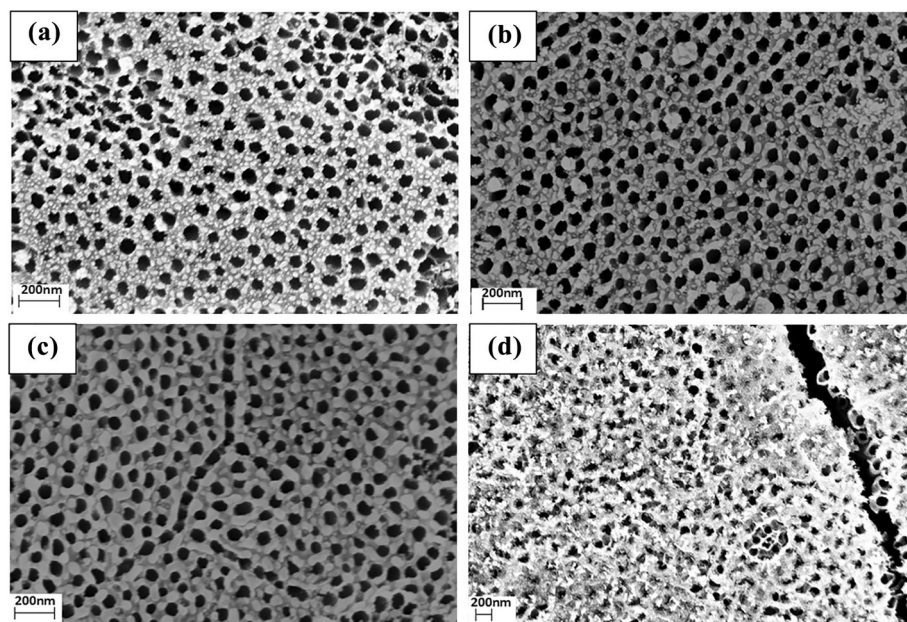

Fig. 3 SEM Images of Ag Nanoparticle-loaded TiO$_2$ Nanotube Arrays with sputtering durations of 30 s, 35 s, 40 s, and 45 s corresponding with (**a**) - (**d**), respectively
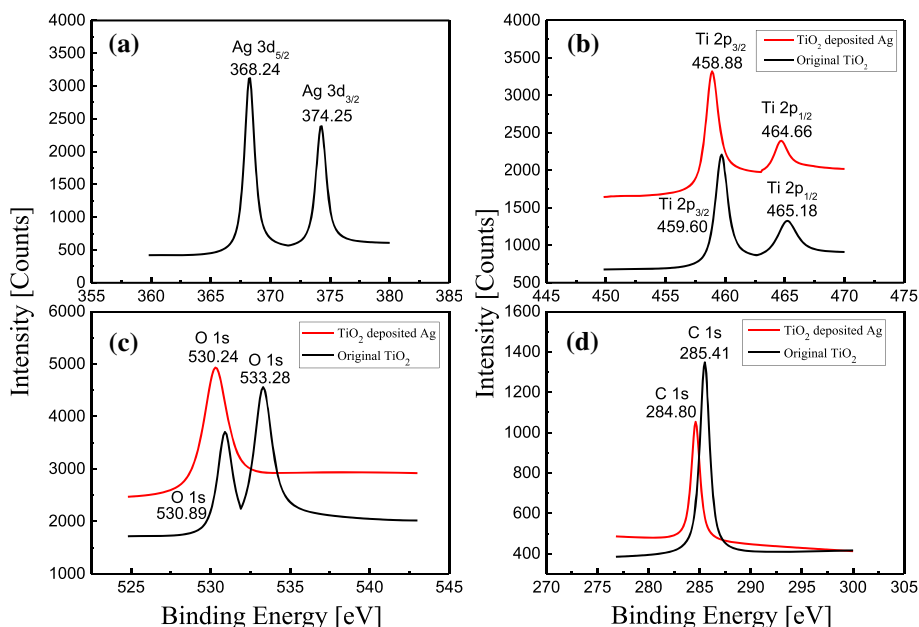
Fig. 4 Photoelectron spectroscopy of the spectra of Ag in (**a**); and the spectroscopies of TiO_2 Nanotubes with/without Ag Deposition in (**b**), (**c**) and (**d**) Measured by XPS, respectively

lattice oxygen to adsorbed oxygen due to the reaction with Ag NPs after deposition.

In Fig. 4d, we detected the spectrum of carbon contamination on TiO_2 nanotube arrays with/without Ag deposition, which were marked with red and black lines respectively. The value of binding energy of carbon contamination was 285.41 eV with the photon number intensity being approximately 1350 counts before deposition. On the contrary, the value of binding energy of carbon contamination was 284.80 eV with the photon number intensity being approximately 1050 counts after Ag deposition, which meant that the value of binding energy and the photon number of carbon was reduced by 0.59 eV and 30% respectively. These results indicated that the amount of carbon contamination was significantly reduced after Ag NPs deposition. In other words, deposition of Ag NPs can reduce contamination of the electrode as well as improve the efficiency of charge transfer. It should be noted that shift of binding energy measured after deposition was approximately 0.8 eV, which was mainly due to shift of carbon.

Therefore, TiO_2 nanotube arrays deposited with Ag NPs can effectively reduce the recombination rate of electrons and holes, and increase conductivity and charge transfer rate of the electrodes compared to TiO_2 nanotube arrays without Ag NPs.

Sensing of Fe^{3+} Ions With/Without Ag NPs Deposition

In order to obtain the experimental results, electrochemical stripping voltammetry was used to detect metallic Fe^{3+}

ions with TiO_2 nanotube arrays without Ag NPs deposition. The concentration of Fe^{3+} ions is set within a range from 10 μg/L to 50 μg/L. Dissolution current's dependence on the voltage when Fe^{3+} ions were detected is shown in Fig. 5. During measurement, when the applied voltage was less than − 0.3 V, the dissolution current kept constant and remained approximately 0 A. When the applied voltage was within a range from − 0.3 V to − 0.16 V, the current dropped rapidly, and the peak reduced approximately from − 1.16 × 10−4 A to − 1.28 × 10−4 A with the Fe^{3+} ions concentration increment being within a range from 10 μg/L to 50 μg/L and with the voltage shifts being within a range from − 0.18 V to − 0.16 V, respectively. The inset shows
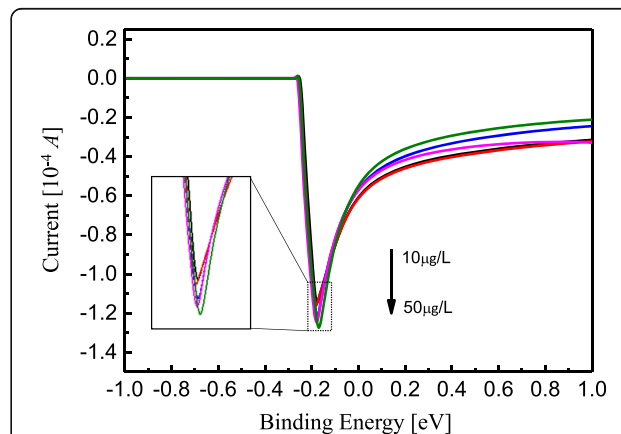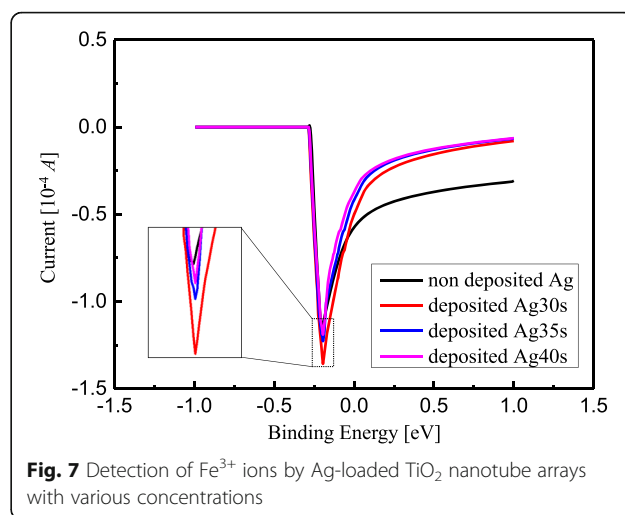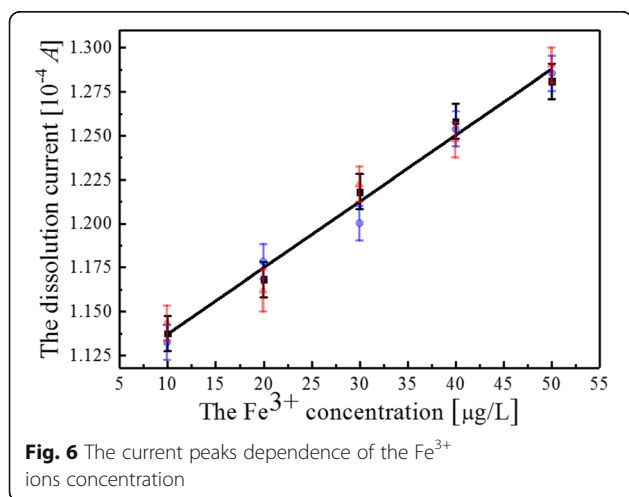

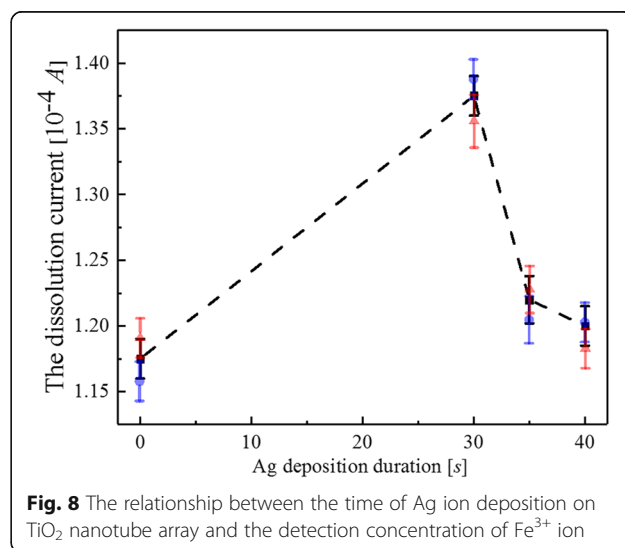**Fig. 5** The dissolve current dependence of the voltage when detected Fe^{3+} ions

current peak's dependence on the applied voltage, as shown in Fig. 5. When the applied voltage V > − 0.16 V, the dissolution current increased exponentially and gradually, and stayed within a range from − 0.2 × 10^{-4} A to − 0.4 × 10^{-4} A. From this result, it can be seen that the peak of the current decreases with increase in Fe^{3+} ion concentration, and that the TiO_2 nanotube array can be used as Fe^{3+} detection sensor.

Dependence of the current peaks in Fig. 5 on Fe^{3+} ions concentration (from 10 μg/L to 50 μg/L) is also summarized in Fig. 6. The solid line is data fitting and is in alignment with linearity in a reasonable manner. Results of the fits can be calculated with $y = 0.00373x + 1.1027$, where y and x represent current and ion concentrations, respectively. This fitting result is sufficient for showing that the minimum detectable Fe^{3+} ion concentration when TiO_2 nanotube arrays without Ag NPs deposition are adopted is 37.3 μA/μg/L. The detection limit of Fe^{3+} ($\delta x = (dy/dx)^{-1} \cdot (1/dy)$) when the TiO_2 arrays are used should be 15.01 nM with consideration of linear range. Here, $dy/dx = 37.3$ μA/μg/L, and $\delta y = 0.01$ μA, $M_{Fe} = 56$, respectively. This result is comparable to that in Ref [25]. In this paper, the extinction ratio A700 nm/A520 nm is linear with the concentration of Fe^{3+} ranging from 40 mM to 80 mM, which can perform sensitive detection of Fe^{3+} ions with a detection limit of 14.82 nM when DTC-PASAu NP-based UV-visible method for on-site and real-time detection of Fe^{3+} in biological samples are adopted.

Next, sensitivity enhancement of Fe^{3+} concentration detection for TiO_2 nanotube arrays with Ag deposition was investigated, with deposition durations being 30s, 35 s, and 40s respectively. The Fe^{3+} concentration was set at 10 μg/L, and the result is shown in Fig. 7. When the applied voltage V was less than − 0.3 V, the dissolution current kept almost constant and was approximately 0 A. When the applied voltage was within a range from − 0.3 V to − 0.2 V, the current dropped

Fig. 7 Detection of Fe^{3+} ions by Ag-loaded TiO_2 nanotube arrays with various concentrations

rapidly to approximately − 1.35 × 10^{-4} A, and when the applied voltage was greater than − 0.2 V, the dissolution current increased exponentially and gradually, and stayed within a range from − 0.08 × 10^{-4}A to − 0.4 × 10^{-4} A. The inset shows current peak's dependence on the applied voltage, as shown in Fig. 7. Dependence of the peaks in Fig. 7 on the Ag NPs deposition with the duration being within a range from 0 s to 40 s is also summarized in Fig. 8, and the solid line presented data fitting. It can be seen that the current reached the maximum value (approximately − 1.38 × 10^{-4} A) when the deposition time of Ag NPs was 30 s. In particular, compared to the value of current before Ag deposition onto TiO_2 nanotube arrays, the value of current increased to approximately − 1.15 × 10^{-4} A, which meant that sensitivity of the Fe^{3+} detection was enhanced by 20% when Ag NPs deposition occurred on TiO_2 surface. Besides, the maximum value of current in the deposition duration of 30 s was considered to be directly related with diameters and

Fig. 6 The current peaks dependence of the Fe^{3+} ions concentration

Fig. 8 The relationship between the time of Ag ion deposition on TiO_2 nanotube array and the detection concentration of Fe^{3+} ion

Ma *et al. Nanoscale Research Letters* (2019) 14:49

Page 7 of 8

uniform distribution of Ag NPs on TiO_2 surface. Consequently, TiO_2 nanotube arrays are characterized by relatively simple fabrication, high sensitivity, and reproducibility compared to other Fe^{3+} detection methods. Moreover, color change of the Ag colloidal solution can be distinguished with naked eyes, which can also be used to directly check whether Fe^{3+} exists in the solution and serves as a strong basis for this research. Therefore, functionalized Ag NPs on well-ordered TiO_2 nanotube arrays provided low-cost, high-selectivity, and sensitivity sensing response for Fe^{3+} with a low limit of detection under ambient conditions. Notably, enhancement of sensitivity of Fe^{3+} detection can also be realized for other Fe^{3+} solutions with different concentrations.

In order to demonstrate the selectivity of TiO_2-Ag NPs for Fe^{3+} ions, competitive experiments were carried out in the presence of other metal ions when surface plasmon resonance (SPR), UV-visible spectrometry, etc. were used. Theoretically, the characteristic peak shift should occur only with the mixed solution of metal ions containing Fe^{3+} ions as indicated in Eqs. (1)–(4). We will focus on the competitive experiments next.

Conclusions

TiO_2 is an important functional material which is not only widely used in UV detectors, photocatalysts, and dye-sensitized solar cells, but also used in important potential applications in ultrasensitive sensors. In this paper, we present a method that utilizes well-aligned TiO_2 nanotube arrays with Ag nanoparticles as voltammetry sensor for highly efficient detection of Fe^{3+} Ion. In the beginning, the anodic oxidation method was adopted to prepare ordered TiO_2 nanotube arrays, followed by functionalized Ag NPs with the ability of iron ions sensing. Then, the spectrums of the TiO_2 nanotube with/without the Ag NPs were compared by XPS, which proved that lattice oxygen in TiO_2 nanotube arrays was released to adsorbed oxygen because of the interaction of Ag NPs. Therefore, when functionalized Ag NPs on nanotube arrays were used, iron ion sensing performed with the anodic stripping voltammetry method was investigated to validate their great potential in becoming heavy metal sensors, which proved that functionalized Ag NPs on well-ordered TiO_2 nanotube arrays provided low-cost, high-selectivity, and sensitivity sensing response for Fe^{3+} with a low limit of detection under ambient conditions. This method creates new possibilities for developing sensors for monitoring of Fe^{3+} in biological samples without any sample pretreatment procedure.

Abbreviations

CB: Conductance band; FWHM: Full wave at half maximum; NALC: N-acetyl-L-cysteine; NPs: Nanoparticles; ROS: Reactive oxygen species; SEM: Scanning electron microscope; Ti: Titanium; VB: Valence band; XPS: X-ray photoelectron spectrometer

Author details

[1]Science and Technology on Electronic Test & Measurement Laboratory, North University of China, No.3, Xue Yuan Road, Taiyuan 030051, Shanxi, China. [2]School of Instrument and Electronics, North University of China, Taiyuan 030051, China.

References

1. Andrews NC (2000) Iron metabolism: iron deficiency and iron overload. Annu Rev Genomics Hum Genet 1:75
2. Aisen P, Wessling-Resnick M, Leibold EA (1999) Iron metabolism. Curr Opin Chem Biol 3:200–206
3. Eisenstein RS (2000) Iron regulatory proteins and the molecular control of mammalian iron metabolism. Annu Rev Nutr 20:627–662
4. Rouault TA (2006) The role of iron regulatory proteins in mammalian iron homeostasis and disease. Nat Chem Biol 2:406
5. Zhang YL, Wang L, Zhang HC et al (2013) Graphitic carbon quantum dots as a fluorescent sensing platform for highly efficient detection of Fe3+ ions. RSC Adv 3:3733–3738
6. Chereddy NR, Thennarasu S, Mandal AB (2013) A highly selective and efficient single molecular FRET based sensor for ratiometric detection of Fe3 + ions. Analyst 138:1334–1337
7. Bhalla V, Sharma N, Kumar N et al (2013) Rhodamine based fluorescence turn-on chemosensor for nanomolar detection of Fe 3+, ions. Sensors Actuators B Chem 178:228–232
8. Tripathy SK, Ju YW, Han CS (2013) Colorimetric detection of Fe(III) ions using label-free gold nanoparticles and acidic thiourea mixture. Sensors Actuators B Chem 181:114–118
9. Velmurugan K, Prabhu J, Tang L et al (2014) A simple chalcone-based fluorescent chemosensor for the detection and removal of Fe3+ ions using a membrane separation method. Anal Methods 6:2883–2888
10. Mehta VN, Kailasa SK, Wu HF (2014) Sensitive and selective colorimetric sensing of Fe3+ ion by using p-amino salicylic acid dithiocarbamate functionalized gold nanoparticles. New J Chem 38:1503–1511
11. Sadrolhosseini AR, Noor AS, Bahrami A et al (2014) Application of polypyrrole multi-walled carbon nanotube composite layer for detection of mercury, lead and iron ions using surface plasmon resonance technique. PLoS One 9:e93962
12. Gao X, Lu Y, He S et al (2015) Colorimetric detection of iron ions (III) based on the highly sensitive plasmonic response of the N -acetyl- l -cysteine-stabilized silver nanoparticles. Anal Chim Acta 879:118–125
13. Yan F, Zheng T, Shi D et al (2015) Rhodamine-aminopyridine based fluorescent sensors for Fe3+, in water: synthesis, quantum chemical interpretation and living cell application. Sensors Actuators B Chem 215: 598–606

14. Zhang C, Cui Y, Li S et al (2016) Microwave assisted one-pot synthesis of graphene quantum dots as highly sensitive fluorescent probes for detection of iron ions and pH value. Talanta 150:54–60

15. Gupta VK, Singh AK, Kumawat LK et al (2016) An easily accessible switch-on optical chemosensor for the detection of noxious metal ions Ni(II), Zn(II), Fe(III) and UO_2 (II). Sensors Actuators B Chem 222:468–482

16. Khan MA , Woo SI , Yang OB (2008) Hydrothermally stabilized Fe(III) doped titania active under visible light for water splitting reaction. International Journal of Hydrogen Energy 33:5345-5351

17. Zhang S, Li J, Zeng M et al (2014) Polymer nanodots of graphitic carbon nitride as effective fluorescent probes for the detection of Fe^{3+} and Cu^{2+} ions. Nanoscale 6:4157–4162

18. Tao L, Xiong Y, Liu H et al (2013) High performance PbS quantum dot sensitized solar cells via electric field assisted in situ chemical deposition on modulated TiO2 nanotube arrays. Nanoscale 6:931–938

19. Yu D, Zhu X, Zhen X, Zhong X, Gui Q, Ye S et al (2014) Facile method to enhance the adhesion of TiO_2 nanotube arrays to ti substrate. ACS Appl Mater Interfaces 6:8001–8005

20. Ge MZ, Cao CY, Li SH, Tang YX, Wang LN, Qi N et al (2016) In situ plasmonic Ag nanoparticle anchored TiO_2 nanotube arrays as visible-light-driven photocatalysts for enhanced water splitting. Nanoscale 8:5226

21. Gao X, Li J, Gollon S, Qiu M, Guan D, Guo X et al (2017) A TiO2 nanotube network electron transport layer for high efficiency perovskite solar cells. Phys Chem Chem Phys 19:4956

22. Masrournia M, Zamani HA, Mirrashid HA et al (2011) Di-tert-butylazodicarboxylate based PVC membrane sensor for Fe(III) ion measurement in pharmaceutical formulation[J]. Mater Sci Eng C 31:574–578

23. Tam TV, Trung NB, Kim HR, et al (2014) One-pot synthesis of N-doped graphene quantum dots as a fluorescent sensing platform for Fe3+ ions detection. Sensors and Actuators B Chemical 202:568-573

24. Jigna RB, Sanjay J, Rakesh KS, Suresh KK (2017) Synthesis of water dispersible fluorescent carbon nanocrystals from syzygium cumini fruits for the detection of Fe^{3+} ion in water and biological samples and imaging of Fusarium avenaceum cells. J Fluoresc 27:125–134

25. Mehta VN, Kailasa SK, Wu HF (2014) Sensitive and selective colorimetric sensing of Fe^{3+} ion by using p-amino salicylic acid dithiocarbamate functionalized gold nanoparticles. New J Chem 38(150320):14

26. Xu JY, Zhou Y, Liu SX, Dong MT, Huang CB (2014) Low-cost synthesis of carbon nanodots from natural products used as a fluorescent probe for the detection of ferrum(III) ions in lake water, Anal. Methods 6:2086–2090

27. Chen YC, Jian YL, Chiu KH et al (2012) Simultaneous speciation of iron(II) and iron(III) by ion chromatography with chemiluminescence detection. Anal Sci 28:795

28. Zhou L, Zhang H, Luan Y, et al (2014) Amplified Detection of Iron Ion Based on Plasmon Enhanced Fluorescence and Subsequently Fluorescence Quenching. Nano-Micro Letters 6:327-334.

29. Diwan U, Kumar A, Kumar V, et al (2013) Solvent viscosity tuned highly selective NIR and ratiometric fluorescent sensing of Fe^{3+} by a symmetric chalcone analogue. Dalton Transactions 42:13889-13896

30. Wu SP, Chen YP, Sung YM (2011) Colorimetric detection of Fe^{3+} ions using pyrophosphate functionalized gold nanoparticles. Analyst 136:1887–1891

31. Masrournia M, Zamani HA, Mirrashid HA et al (2011) Di-tert-butylazodicarboxylate based PVC membrane sensor for Fe(III) ion measurement in pharmaceutical formulation. Mater Sci Eng C 31:574–578

32. Bagheri H, Gholami A, Najafi A (2000) Simultaneous preconcentration and speciation of iron(II) and iron(III) in water samples by 2-mercaptobenzimidazole-silica gel sorbent and flow injection analysis system. Analytica Chimica Acta 424:233-242

33. Wang D, Wang L, Dong X et al (2012) Chemically tailoring graphene oxides into fluorescent nanosheets for Fe 3+, ion detection. Carbon 50:2147–2154

34. Chereddy NR, Suman K, Korrapati PS et al (2012) Design and synthesis of rhodamine based chemosensors for the detection of Fe^{3+} ions. Dyes Pigm 95:606–613

35. Choi YW, Park GJ, Na YJ, et al (2014) A single schiff base molecule for recognizing multiple metal ions: A fluorescence sensor for Zn(II) and Al(III) and colorimetric sensor for Fe(II) and Fe(III). Sensors and Actuators B Chemical 194:343-352

36. Chen L, Li J, Chen L (2014) Colorimetric Detection of Mercury Species Based on Functionalized Gold Nanoparticles. ACS Applied Materials & Interfaces 6:15897-15904

37. Taketoshi M, Yasuyuki S, Kim Y et al (2009) The electronic structure of oxygen atom vacancy and hydroxyl impurity defects on titanium dioxide (110) surface. J Chem Phys 130:124502

38. Li N, Zhang D, Qian Z et al (2016) Combining localized surface plasmon resonance with anodic stripping voltammetry for heavy metal ion detection. Sensors Actuators B Chem 231:349–356

39. Ma Z, Gao J, Wu X et al (2018) Preparation of well-aligned TiO2 nanotubes with high length-diameter aspect ratio by anodic oxidation method. J Nanosci Nanotechnol 18:5810–5816